iScience

CellPress
OPEN ACCESS

Article

Highly efficient generation of GV/m-level terahertz pulses from intense femtosecond laser-foil interactions

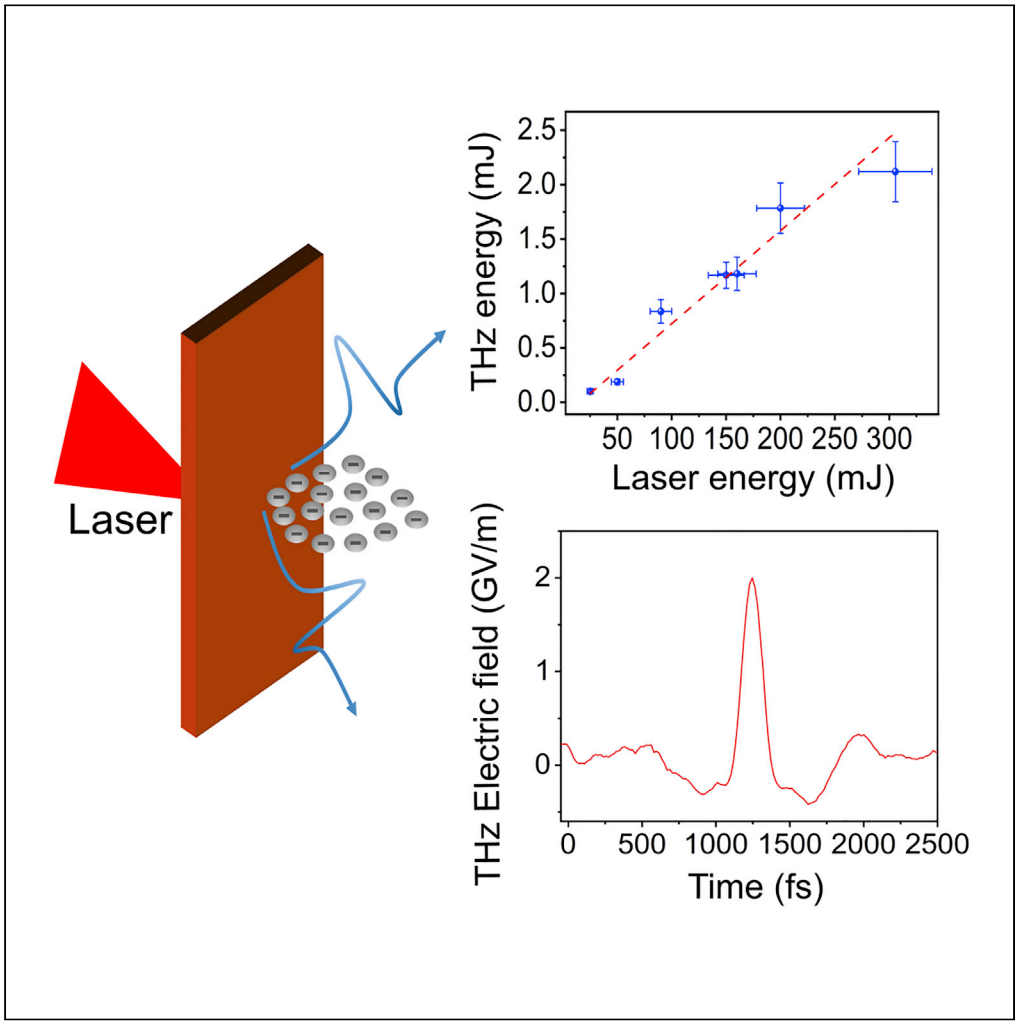

Hong-Yi Lei, Fang-Zheng Sun, Tian-Ze Wang, ..., Jing-Long Ma, Guo-Qian Liao, Yu-Tong Li

gqliao@iphy.ac.cn (G.-Q.L.)
ytli@iphy.ac.cn (Y.-T.L.)

Highlights

Ultraintense laser-foil interactions generate a 2.1-mJ strong terahertz pulse

Nearly 1% generation efficiency originates from optimized laser-plasma conditions

2-GV/m high THz fields induce absorption bleaching and impact ionization

Lei et al., iScience 25, 104336
May 20, 2022
https://doi.org/10.1016/j.isci.2022.104336

iScience

CellPress
OPEN ACCESS

Article

Highly efficient generation of GV/m-level terahertz pulses from intense femtosecond laser-foil interactions

Hong-Yi Lei,[1,2] Fang-Zheng Sun,[1,2] Tian-Ze Wang,[1] Hao Chen,[1,2] Dan Wang,[1,2] Yan-Yu Wei,[1,2] Jing-Long Ma,[1] Guo-Qian Liao,[1,3,5,*] and Yu-Tong Li[1,2,3,4,*]

SUMMARY

The terahertz radiation from ultraintense laser-produced plasmas has aroused increasing attention recently as a promising approach toward strong terahertz sources. Here, we present the highly efficient production of millijoule-level terahertz pulses, from the rear side of a metal foil irradiated by a 10-TW femtosecond laser pulse. By characterizing the terahertz and electron emission in combination with particle-in-cell simulations, the physical reasons behind the efficient terahertz generation are discussed. The resulting focused terahertz electric field strength reaches over 2 GV/m, which is justified by experiments on terahertz strong-field-driven nonlinearity in semiconductors.

INTRODUCTION

In the past few decades, terahertz science has become a rapidly developing research field (Tonouchi, 2007). The unique frequency range of the terahertz radiation brings the possibility to induce novel phenomena in various material systems, to name a few, the ferroelectric phase transition in perovskite materials (Li et al., 2019), the terahertz-induced superconductivity in graphene (Yang et al., 2019), and the terahertz-assisted chemistry (LaRue et al., 2015). The strong terahertz field also demonstrates tempting potential in particle acceleration (Nanni et al., 2015; Zhang et al., 2018), high harmonic generation (Kovács et al., 2012), and nonlinear carrier dynamics in semiconductors (Tarekegne et al., 2017). Intense terahertz radiation sources at GV/m-level field strength are much desired for these applications and further development of extreme terahertz science.

Conventionally, strong terahertz-pulsed sources are based on large-scale electron accelerators (Carr et al., 2002; Wu et al., 2013; Pacey et al., 2019) and ultrafast laser systems (Stojanovic and Drescher, 2013). Although the accelerator-based sources can produce powerful terahertz radiation with a tunable frequency spectrum, the difficulty in producing short-duration energetic electron bunches makes it challenging to increase the terahertz energy, and the rareness of electron accelerators has limited their accessibility. Ultrafast laser-based terahertz sources depend mostly on optical rectification from nonlinear crystals like lithium niobate (LN) (Fülöp et al., 2014) and organic crystals like DSTMS (Vicario et al., 2014) or BNA (Roeder et al., 2020). Great progress have been made, *e.g.*, mJ-level GV/m terahertz pulses have been produced from LN (Zhang et al., 2021) and DSTMS (Vicario et al., 2014) with a generation efficiency of the order of 1%. However, large-size high-quality crystals are needed to further increase the terahertz energy, which brings realistic limitation.

Laser-induced plasmas show the potential as damage-free medium for producing terahertz radiation (Hamster et al., 1993; Cook and Hochstrasser, 2000). The air-plasma-based terahertz sources have been intensively studied. However, the terahertz radiation energy tends to saturate when increasing the pump laser energy and the terahertz energy is limited to microjoule level with the commonly used near-infrared laser systems (Clerici et al., 2013; Kuk et al., 2016). The terahertz sources based on ultraintense laser-solid interactions, by contrast, show potential on generating high terahertz energy, and no sign of saturation has been reported (Liao and Li, 2019a). Intense terahertz radiation has been observed from both the front and the rear side of solid targets irradiated by an intense laser pulse (Li et al., 2011, 2012; Gopal et al., 2012, 2013; Liao et al., 2015, 2016; Jin et al., 2016). For the terahertz radiation emitted from the foil rear side, 200-mJ-level and terawatt-scale terahertz pulses have been demonstrated at the powerful picosecond

[1]Beijing National Laboratory for Condensed Matter Physics, Institute of Physics, Chinese Academy of Sciences, Beijing 100190, China

[2]School of Physical Sciences, University of Chinese Academy of Sciences, Beijing 100049, China

[3]Songshan Lake Materials Laboratory, Dongguan 523808, Guangdong, China

[4]Collaborative Innovation Center of IFSA (CICIFSA), Shanghai Jiao Tong University, Shanghai 200240, China

[5]Lead contact

*Correspondence: gqliao@iphy.ac.cn (G.-Q.L.), ytli@iphy.ac.cn (Y.-T.L.)

https://doi.org/10.1016/j.isci.2022.104336

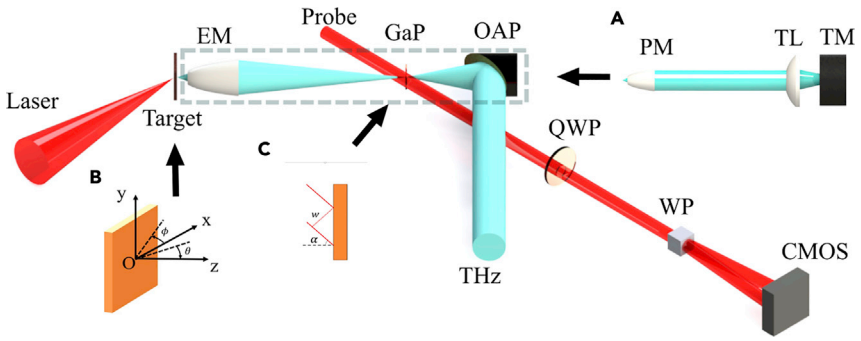

Figure 1. Experimental setup

The focused laser pulse irradiates on the 10-μm thick copper foil target, producing terahertz radiation from the target rear surface. The laser focusing OAP is not presented. The terahertz radiation is collected and focused by an ellipsoidal mirror and then re-collimated by an OAP. Terahertz time-domain waveform was measured by the GaP crystal (EO crystal) using non-collinear spatially encoded electro-optic sampling method with a balanced detection setup. The probe laser pulse is split inside the vacuum chamber from the main laser beam. EM: Ellipsoidal mirror. QWP: Quarter wave plate. WP: Wollaston prism. THz: terahertz beam. CMOS: the probe laser detection camera. The pyroelectric energy detector, which is placed outside the target chamber, is not presented in the figure. Insert: (A) Schematic setup showing measurements of the terahertz angular distribution. This setup replaces the optical components in the gray rectangle during the angular distribution measurements. The ellipsoidal mirror was replaced with a parabolic mirror (PM). The collimated terahertz radiation was focused by a TPX lens (TL) and detected by a terahertz camera (TM). The camera was placed in front of the nominal terahertz focus to record the terahertz spatial distribution.
(B) Schematic presentation of the coordinate at the target rear. ϕ is the azimuthal angle in the xOy plane.
(C) Schematic presentation of the spatial-time mapping on the GaP crystal for the non-collinear spatial encoding method, where w is the probe beam width and α is the probe incidence angle.

laser facility (Liao et al., 2019b, 2020). In the femtosecond laser experiments reported previously, the terahertz radiation energy detected was usually hundreds of microjoules (Liao et al., 2015; Herzer et al., 2018) with the electric field strength at the level of ~0.3 GV/m, at the laser-to-terahertz energy conversion efficiency in the level of ~0.1%.

In this paper, we report the generation of 2.1-mJ terahertz radiation from intense laser-foil interactions by utilizing a table-top 10-TW femtosecond laser system, and correspondingly, at a laser-to-terahertz conversion efficiency of ~0.7%. By characterizing the terahertz radiation properties and measuring the hot electrons at the target rear side, the terahertz radiation is attributed to the coherent transition radiation of energetic electrons crossing the target-vacuum boundary. Particle-in-cell simulations are performed to understand the high conversion efficiency. Preliminary strong-field terahertz application experiments verify the available peak terahertz field strength over 2 GV/m.

RESULTS AND DISCUSSION

Terahertz characterization

The experiment was carried out using the 10-TW Ti:sapphire femtosecond laser system at the Institute of Physics, Chinese Academy of Sciences. The laser system is able to deliver laser energy of 300 mJ with center wavelength of 800 nm, pulse duration of 30 fs, and 10-Hz repetition rate. Single-shot mode of the laser was used in the experiment. The schematical experimental setup is shown in Figure 1. The 30-fs laser pulse was focused on a 10-μm thick copper foil by an off-axis parabola (OAP) at an incidence angle of 45° (see Method details). The maximum laser intensity on target was about 1×10^{19} W/cm^2 at the best laser focal spot of less than 8-μm diameter. The terahertz radiation emitted from the target rear side was collected with a customized ellipsoidal mirror, and then the terahertz energy was measured by a pyroelectric detector. The terahertz energy increases approximately linearly with the laser energy, as shown in Figure 2A. The maximum terahertz energy measured is ~2.1 mJ at the 300-mJ laser energy pump, corresponding to an energy conversion efficiency of ~0.7%. Measurements show the relative shot-to-shot fluctuation of terahertz energy is within 10%.

The time-domain waveform of terahertz radiation was measured with the non-collinear spatially encoded electro-optic (EO) sampling method (Shan et al., 2000) (see Method details). The EO sampling signals

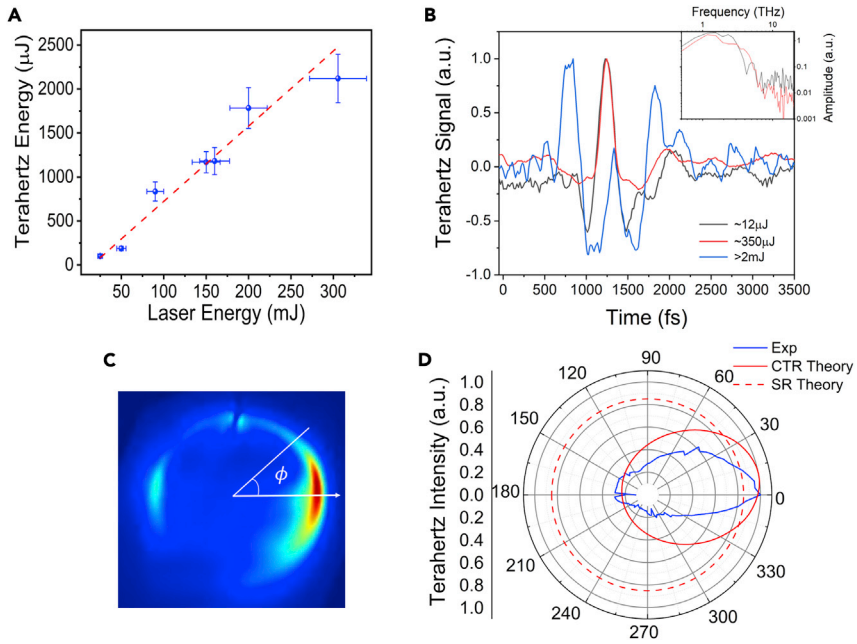

Figure 2. Terahertz characterization

(A) Terahertz radiation energy as a function of the laser energy, the red dashed line shows the linear fit of the result.

(B) The time-domain waveforms measured at different terahertz energies are presented. Here, we note that the blue curve is the time-domain waveform measured using a 50 μm GaP crystal when terahertz energy was over 2 mJ. The insert figure is the corresponding frequency spectrum of the attenuated terahertz radiation at 12 μJ and 350 μJ.

(C) Spatial profile of the terahertz radiation collected by a parabolic mirror.

(D) Integrated terahertz angular distribution and the comparison with the theoretical calculation.

measured at different terahertz energies are shown in Figure 2B. At the low and moderate terahertz energy, measurements show similar quasi-half-cycle terahertz waveforms, whose pulse duration (FWHM) are measured to be about 150 fs. The terahertz frequency spectrum can be obtained by performing Fournier transform of the time-domain waveform. The broadband terahertz spectrum extends to about 6 THz, which is close to the detection limit by the EO crystal used (Casalbuoni et al., 2008). The spectral maximum locates at ~1.5 THz, which is due to the small oscillations around the main peak. At the high terahertz energy, multiple peaks appear in the EO signal, which is resulted from the over-rotation effect at high fields (Bell and Hilke, 2020). According to the EO measurement, the terahertz field strength at the 12-μJ terahertz energy is retrieved to be ~0.10 GV/m. Considering the relation of the energy and the electric field strength, the terahertz peak field strength can reach ~1.36 GV/m at the maximum terahertz energy of ~2.1 mJ.

To measure the terahertz focal spot, the collected terahertz radiation was relayed outside the target chamber and then refocused by an OAP to a microbolometer camera. The area of the focal spot is measured to be about 1.6 mm^2 (See also Figure S1). Measurements show that the terahertz pulse duration and focal spot do not vary much at different terahertz energies. Based on the measured terahertz energy, pulse duration, and focal spot, the peak terahertz field strength is calculated to be ~2.55 GV/m (Zhang et al., 2021), which is larger than the field strength measured by the EO sampling method. This may be due to the complicated polarization of the terahertz radiation (Woldegeorgis et al., 2018). Given the fact that a terahertz polarizer was not used before the EO crystal in the experiment, the measured field strength is the projection of the total field strength on the crystal axis. As a result, the field strength measured by the EO sampling is smaller than the evaluated one.

In order to measure the angular distribution of the terahertz radiation, we replaced the ellipsoidal mirror with a parabolic mirror (Insert (a) in Figure 1). The collected terahertz radiation was converted into a collimated beam, and then focused by a TPX lens. The camera was placed in front of the focal spot to get the spatial profile of the terahertz radiation, as shown in Figure 2C. The terahertz intensity integrated along the

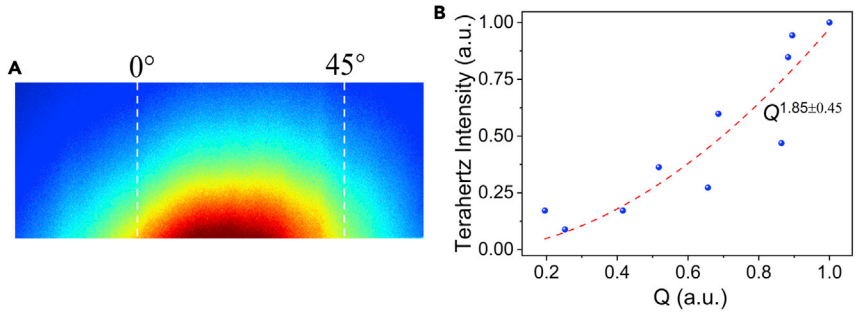

Figure 3. Electron measurements

(A) Typical image recorded on the image plate (IP).

(B) Dependence of terahertz radiation energy on the measured electron charge.

azimuthal angle (ϕ in Figure 2C) is used to approximately represent its angular distribution, showing an azimuthally non-symmetric character, as shown in Figure 2D.

Terahertz generation mechanism

Intense laser-plasmas interactions can generate numerous hot electrons (Wilks and Kruer, 1997). The hot electrons transport to the target rear and can induce terahertz radiation via coherent transition radiation (CTR) (Schroeder et al., 2004; Liao et al., 2016). The coherent transition radiation energy in unit angular frequency and unit solid angle can be expressed as

$$\frac{dW_{CTR}}{d\omega d\Omega} \approx \frac{dW_e}{d\omega d\Omega} N_e (N_e - 1) |F_{CTR} D|^2, \qquad \text{(Equation 1)}$$

where $\frac{dW_e}{d\omega d\Omega}$ is the transition radiation from a single electron, N_e is the number of electrons, F_{CTR} is the bunch form factor, and D is the diffraction factor. As the number of electrons produced in laser-solid interactions is usually very large, $W_{CTR} \propto N_e^2 \propto Q^2$, where Q is the total charge of the electron beam.

Another possible terahertz generation mechanism is the sheath radiation (SR) induced by the transient sheath field associated with ion acceleration at the target rear (Gopal et al., 2013; Liao et al., 2020). During ion acceleration process, the electron-ion sheath behaves like a time-varying transient current. The sheath radiation energy in unit angular frequency and unit solid angle can be expressed as (Liao et al., 2020).

$$\frac{d^2 W_{SR}}{d\omega d\Omega} = \frac{q^2 c_s^2}{4\pi^3 \varepsilon_0 c^3} |F_{SR}|^2 \sin^2 \theta, \qquad \text{(Equation 2)}$$

where q is the net charge in the sheath, c_s is the ion sound velocity, c is the speed of light, and F_{SR} is the form factor. The formula indicates that the sheath radiation has a symmetric angular distribution in the azimuthal direction with respect to the target normal.

In order to confirm whether the terahertz radiation is mainly produced via CTR by hot electrons, we measured the terahertz radiation and the electron charge at the target rear by varying the laser intensity. In the experiment, we moved the position of the laser OAP along the laser axis to vary the laser intensity on the target, while keeping a fixed position for the laser spot on the target and accordingly the unchanged terahertz collection efficiency. An image plate (IP) stack was placed at the rear of the target to detect electrons (Tanaka et al., 2005). Figure 3A shows the typical signal recorded on the IP stack. The electron bunch was observed between the target normal direction and the laser propagation direction, with a divergence angle of ~30°(FWHM). The charge and temperature of the electron bunch can be evaluated according to the signals measured by the IP stack (see Method details). Figure 3B shows the terahertz radiation energy as a function of the measured electron charge. Fitting gives $W \propto Q^{1.85 \pm 0.45}$, which indicates that the terahertz radiation observed in our experiment is the coherent emission by electrons. For the specific shot taken at the laser energy of 90 mJ, the electron charge was retrieved to be ~28 nC and the electron temperature was about 600 keV, and accordingly, corresponding to a laser-to-electron energy conversion efficiency of ~18.6%.

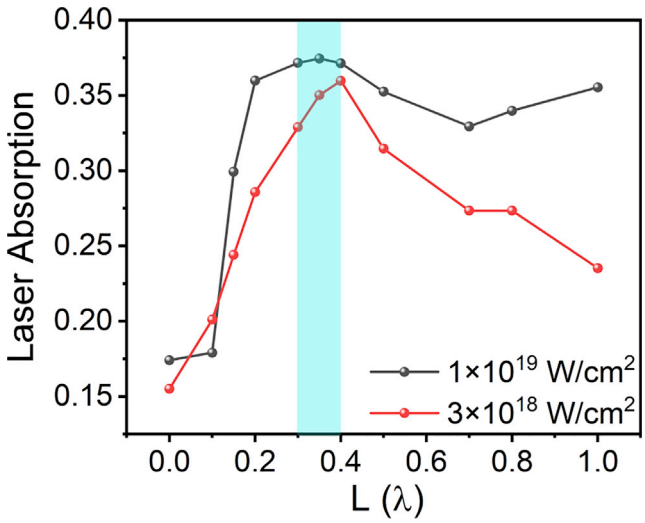

Figure 4. PIC simulations

PIC simulated laser absorption efficiency as a function of the plasma density scale length *L*. The cyan area indicates the plasma density scale length range in the experiment.

Given the fact that the CTR and SR have different angular distributions, one can identify the terahertz generation mechanism by comparing the experimentally measured and theoretically calculated terahertz spatial distribution. According to the measured electron beam profile and electron temperature, the angular distribution of CTR by electrons is calculated numerically, as shown by the red solid curve in Figure 2D. The calculated non-symmetric distribution is in general accord with the experimental observation. The terahertz energy in the collection solid angle is calculated to be 1.0 mJ, which is comparable to the experimentally detected terahertz energy of ~0.84 mJ driven by the 90-mJ laser pulse. The good agreement of the theoretical calculations and experimental observations convinces us that the terahertz radiation observed in the experiment is mainly generated by the CTR of hot electrons, rather than the SR, which is also consistent with our previous experiment (Liao et al., 2016).

Discussion on the high terahertz generation efficiency

In our experiment, a nearly 1% laser-to-terahertz energy conversion efficiency is obtained, which can be qualitatively explained. The terahertz radiation conversion efficiency can be divided into two parts, the laser absorption efficiency, $\eta_{\text{Laser-e}}$, and the efficiency from hot electrons to terahertz radiation, $\eta_{\text{e-THz}}$. $\eta_{\text{e-THz}}$ depends largely on the number and temperature of hot electrons. $\eta_{\text{Laser-e}}$ depends on the laser intensity, incidence angle, and the plasma density distribution. These parameters also determine the laser absorption mechanisms. Especially, the laser contrast can largely affect the laser absorption efficiency by the induced plasma density scale length *L* (Ping et al., 2008; Cui et al., 2013). In our experiment, the typical laser contrast was about 2.0×10^{-8} in 20 ps and a prepulse of $\sim 5\times10^{-4}$ arrived at ~12 ps before the main laser pulse. This prepulse is strong enough to ionize the target and a preplasma can be formed before the main pulse arrives. To evaluate *L* in our experiment, a hydrodynamics fluid simulation using the MULTI code is performed (Ramis et al., 2012), showing *L* is between 0.3λ and 0.4λ at the prepulse intensity between 1×10^{15} W/cm^2 and 5×10^{15} W/cm^2. At this density scale length, the electron heating mechanism could be resonant absorption or J×B heating. Considering that the electrons measured in the experiment emit between the target normal and the laser propagation direction but slightly closer to the target normal direction, both heating mechanisms exist and the resonant absorption contributes more under our experiential condition. For the resonant absorption process, there exists an optimal laser incidence angle θ_m for a specific *L*. $\theta_m = \arcsin\left[0.8\left(\frac{\omega L}{c}\right)^{-\frac{1}{3}}\right]$, where ω is the angular frequency of the laser and *c* is the speed of light (Wilks and Kruer, 1997). For the *L* in the experiment, θ_m is 36°–40°. The laser incidence angle (45°) in our experiment is rationally close to θ_m. Thus, high laser absorption efficiency is expected.

In order to confirm this high laser absorption efficiency, we have performed two-dimensional particle-in-cell (PIC) simulation using the EPOCH code (Arber et al., 2015) (see Method details). Figure 4 shows the

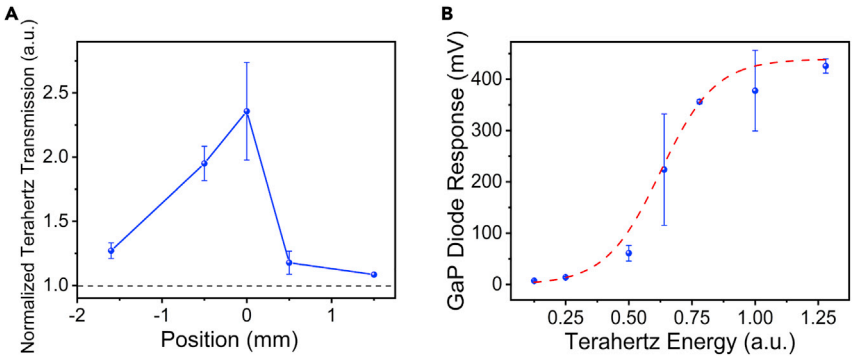

Figure 5. Demonstrative experiments

(A) Transmitted terahertz energy versus the position of the doped silicon wafer. The best terahertz focus locates at 0 mm. The dash line represents the measured terahertz signal when the sample is far away from the terahertz focus.

(B) Output signal of GaP diode as a function of the terahertz energy.

laser absorption efficiency as a function of plasma density scale in the range of $L = 0–1\lambda$. For the laser intensity of 1×10^{19}W/cm^2, the maximum laser absorption of ~38% occurs at $L = 0.4\ \lambda$. The rather large absorption efficiency at $L \sim 0.4\ \lambda$ is partially because the incidence angle is close to θ_m. In our experiment, L is between $0.3\ \lambda$ and 0.4λ, which fall exactly in the optimal range of plasma density scale lengths given by simulations. The simulation at laser intensity of 3×10^{18}W/cm^2 is performed to confirm the optimal plasma density scale range keeps unchanged in our experiment. Because the forward propagating electrons contain about half of the absorbed laser energy, the maximum energy conversion efficiency from the laser to forward electron at the target rear is evaluated to be ~17.9%, sufficiently close to the experimentally measured value of 18.6%. Consequently, the high laser-to-terahertz energy conversion efficiency can be mainly attributed to the high laser absorption efficiency at an appropriate plasma density scale.

It is enlightening to compare with our previous experiment (Liao et al., 2016), where a laser-to-terahertz efficiency of ~0.02% was obtained at the laser incidence angle of 54° and the plasma density scale length of about $3\ \lambda$ (See also Figure S2 and Table S1). Theoretical analysis and PIC simulations show those parameters of the previous experiment are very unfavorable for the efficient resonant absorption, which suppress the generation of fast electrons. It implies the importance of appropriate laser-plasma configurations. The terahertz generation efficiency could be improved further by optimizing the laser-plasma parameters or using specially structured targets that enhance the laser absorption significantly (Mondal et al., 2017).

Terahertz application demonstrative experiments

In order to demonstrate the capability of the intense terahertz radiation obtained in our experiment, we performed two demonstrative experiments concerning polarization-independent nonlinear response of semiconductors driven by strong terahertz fields.

The first demonstration was on the terahertz nonlinear transmission of doped silicon. In this experiment, about 0.43-mJ THz radiation was focused by an OAP, resulting in peak terahertz field strength of ~1.14 GV/m at the best focus. Similar to the conventional z-scan technique, a doped silicon wafer was put near the terahertz focus, with adjustable position along the terahertz beam axis. A large-aperture pyroelectric detector was used to measure the terahertz energy transmitting the silicon wafer. Figure 5A shows the measured terahertz transmission as a function of the sample position. The terahertz transmission is enhanced when the sample is placed near the terahertz focus, *i.e.*, the terahertz field on the sample gets strong. This so-called nonlinear terahertz absorption bleaching phenomenon can be explained by the intervalley scattering between the X valley and the L valley in the conduction band of the doped silicon (Hebling et al., 2010). At strong terahertz irradiation, the terahertz field-accelerated electrons in the lower X valley can interact with phonons and be scattered to the higher L valley, where the electrons have a higher effective mass, and thus reducing the mobility and the conductivity of the silicon, resulting in an enhanced terahertz transmission. Intervalley scattering rate is proportional to the velocity of the electron (Yu and Cardona, 2010). To achieve a specific intervalley scattering rate and accordingly the same terahertz transmission enhancement, a higher terahertz field is required for the shorter duration terahertz radiation. In the

previous similar experiment, the ~1-ps, 0.25-GV/m terahertz pulse produced from the LN crystal results in an enhancement of terahertz transmission by a factor of 2.3 (Zhang et al., 2021). The terahertz field strength for the ~150-fs terahertz radiation in our current experiment is evaluated to be ~1.09 GV/m (see Method details), comparable to the calculated value 1.14 GV/m.

Another experiment demonstrated the terahertz-driven carrier multiplication in a GaP diode. The terahertz radiation was focused on the diode, and the voltage signal was recorded by an oscilloscope. As shown in Figure 5B, a strong voltage signal is observed. It exponentially increases with the terahertz energy and then saturates when further increasing the terahertz energy exceeding ~0.8 mJ. As the terahertz photon energy is much lower than the bandgap of GaP (~2.24eV), this phenomenon is attributed to the strong terahertz electric-field-induced impact ionization (Hirori et al., 2011). Ionized electrons in the impurities are accelerated by the strong terahertz field and scattered by phonons to produce a lower energy electron and an e-h pair. The generated electrons can be further accelerated by the terahertz field, resulting in an exponential response. The saturation observed in our experiment may be due to the enhanced e-h scattering and electron redistribution at the sufficiently high electron concentration (Hirori et al., 2011). Compared with previously reported experiments where the LN-based picosecond terahertz radiation induces the impact ionization in the narrow-gap superlattice (Ouyang et al., 2021), the electric field strength for the short-duration terahertz radiation presented here should be much larger than those used in previous experiments.

Conclusion

In summary, the generation of terahertz radiation from ultraintense femtosecond laser-foil interactions is investigated. A 2.1-mJ, single-cycle, broadband terahertz pulse with a 0.7% laser-to-terahertz energy conversion efficiency is obtained. Supported by electron measurements together with PIC simulations, the terahertz generation mechanism is clarified to be coherent transition radiation by laser-accelerated hot electrons, and the high generation efficiency is attributed qualitatively to the high laser absorption at an appropriate plasma condition. Experiments performed on the terahertz-driven nonlinearity demonstrate the availability of GV/m-level terahertz field strength. Such an intense terahertz radiation source will offer a unique pump for various ambitious applications such as the ultrafast control over matter and compact electron acceleration.

Limitation of the study

The laser and target parameter scanning in the current experiment is limited, like the laser pulse duration, incidence angle and contrast, target material and thickness *etc.* To further optimize the terahertz generation, further studies with more laser-target parameters are required. The terahertz source is operated currently at the single-shot mode, and its repetition rate and stability can be improved by employing the high-repetition-rate target delivery and positioning systems in future.

STAR★METHODS

Detailed methods are provided in the online version of this paper and include the following:

- KEY RESOURCES TABLE
- RESOURCE AVAILABILITY
  - Lead contact
  - Materials availability
  - Data and code availability
- EXPERIMENTAL MODEL AND SUBJECT DETAILS
- METHOD DETAILS
  - Terahertz waveform measurement
  - Electron measurement
  - Estimation of terahertz field strength using terahertz-induced absorption bleaching
  - Simulation setup
- QUANTIFICATION AND STATISTICAL ANALYSIS

SUPPLEMENTAL INFORMATION

Supplemental information can be found online at https://doi.org/10.1016/j.isci.2022.104336.

ACKNOWLEDGMENTS

The authors would like to thank Bao-Long Zhang and Chen Ouyang for meaningful discussion and sharing data of the LN terahertz source; thank Shao-Jun Wang for helping with the MULTI hydrodynamic simulations; thank Yu-Feng Dong and Yi-Hang Zhang for meaningful discussion on electron data processing. This work is supported by the National Natural Science Foundation of China (Grant Nos. 92050106, 12122415, 12175306 and 11827807), the National Key R&D Program of China (Grant Nos. 2021YFA1400204 and 2021YFA1601700), and the Strategic Priority Research Program of the Chinese Academy of Sciences (Grant No. XDA25010000).

AUTHOR CONTRIBUTIONS

G.Q.L. conceived and designed the experiment. H.Y.L., F.Z.S., T.Z.W., D.W., Y.Y.W., and G.Q.L. performed the experiment. J.L.M. maintained the laser system. H.Y.L. analyzed the data in consultation with G.Q.L. The manuscript was prepared by H.Y.L., G.Q.L., and Y.T.L., and discussed and commented by all authors. All the work was done under the supervision of G.Q.L. and Y.T.L.

DECLARATION OF INTERESTS

The authors declare no competing interests.

Received: August 19, 2021
Revised: April 6, 2022
Accepted: April 27, 2022
Published: May 20, 2022

REFERENCES

Arber, T.D., Bennett, K., Brady, C.S., Lawrence-Douglas, A., Ramsay, M.G., Sircombe, N.J., Gillies, P., Evans, R.G., Schmitz, H., Bell, A.R., and Ridgers, C.P. (2015). Contemporary particle-in-cell approach to laser-plasma modelling. Plasma Phys. Contr. Fusion *57*, 113001. https://doi.org/10.1088/0741-3335/57/11/113001.

Bell, G., and Hilke, M. (2020). Polarization effects of electro-optic sampling and over-rotation for high field THz detection. J. Infrared, Millim. Terahertz Waves *41*, 880–893. https://doi.org/10.1007/s10762-020-00724-z.

Carr, G.L., Martin, M.C., McKinney, W.R., Jordan, K., Neil, G.R., and Williams, G.P. (2002). High-power terahertz radiation from relativistic electrons. Nature *420*, 153–156. https://doi.org/10.1038/nature01175.

Casalbuoni, S., Schlarb, H., Schmidt, B., Schmüser, P., Steffen, B., and Winter, A. (2008). Numerical studies on the electro-optic detection of femtosecond electron bunches. Phys. Rev. Spec. Top. Accel. Beams *11*, 072802. https://doi.org/10.1103/physrevstab.11.072802.

Clerici, M., Peccianti, M., Schmidt, B.E., Caspani, L., Shalaby, M., Giguere, M., Lotti, A., Couairon, A., Legare, F., Ozaki, T., et al. (2013). Wavelength scaling of terahertz generation by gas ionization. Phys. Rev. Lett. *110*, 253901. https://doi.org/10.1103/physrevlett.110.253901.

Cook, D.J., and Hochstrasser, R.M. (2000). Intense terahertz pulses by four-wave rectification in air. Opt. Lett. *25* (16), 1210–1212. https://doi.org/10.1364/ol.25.001210.

Cui, Y.Q., Wang, W.M., Sheng, Z.M., Li, Y.T., and Zhang, J. (2013). Laser absorption and hot electron temperature scalings in laser–plasma interactions. Plasma Phys. Contr. Fusion *55*, 085008. https://doi.org/10.1088/0741-3335/55/8/085008.

Fülöp, J.A., Ollmann, Z., Lombosi, C., Skrobol, C., Klingebiel, S., Pálfalvi, L.L., Krausz, F., Karsch, S., and Hebling, J. (2014). Efficient generation of THz pulses with 0.4 mJ energy. Opt. Express *22* (17), 20155–20163. https://doi.org/10.1364/oe.22.020155.

Gopal, A., Herzer, S., Schmidt, A., Singh, P., Reinhard, A., Ziegler, W., Brommel, D., Karmakar, A., Gibbon, P., Dillner, U., et al. (2013). Observation of gigawatt-class THz pulses from a compact laser-driven particle accelerator. Phys. Rev. Lett. *111*, 074802. https://doi.org/10.1103/physrevlett.111.074802.

Gopal, A., May, T., Herzer, S., Reinhard, A., Minardi, S., Schubert, M., Dillner, U., Pradarutti, B., Polz, J., Gaumnitz, T., et al. (2012). Observation of energetic terahertz pulses from relativistic solid density plasmas. New J. Phys. *14*, 083012. https://doi.org/10.1088/1367-2630/14/8/083012.

Hamster, H., Sullivan, A., Gordon, S., White, W., and Falcone, R.W. (1993). Subpicosecond, electromagnetic pulses from intense laser-plasma interaction. Phys. Rev. Lett. *71*, 2725–2728. https://doi.org/10.1103/physrevlett.71.2725.

Hebling, J., Hoffmann, M.C., Hwang, H.Y., Yeh, K.L., and Nelson, K.A. (2010). Observation of nonequilibrium carrier distribution in Ge, Si, and GaAs by terahertz pump–terahertz probe measurements. Phys. Rev. B *81*, 035201. https://doi.org/10.1103/physrevb.81.035201.

Herzer, S., Woldegeorgis, A., Polz, J., Reinhard, A., Almassarani, M., Beleites, B., Ronneberger, F., Grosse, R., Paulus, G.G., Hübner, U., et al. (2018). An investigation on THz yield from laser-produced solid density plasmas at relativistic laser intensities. New J. Phys. *20*, 063019. https://doi.org/10.1088/1367-2630/aaada0.

Hirori, H., Shinokita, K., Shirai, M., Tani, S., Kadoya, Y., and Tanaka, K. (2011). Extraordinary carrier multiplication gated by a picosecond electric field pulse. Nat. Commun. *2*, 594. https://doi.org/10.1038/ncomms1598.

Jin, Z., Zhuo, H.B., Nakazawa, T., Shin, J.H., Wakamatsu, S., Yugami, N., Hosokai, T., Zou, D.B., Yu, M.Y., Sheng, Z.M., and Kodama, R. (2016). Highly efficient terahertz radiation from a thin foil irradiated by a high-contrast laser pulse. Phys. Rev. E *94*, 033206. https://doi.org/10.1103/physreve.94.033206.

Kovács, K., Balogh, E., Hebling, J., Toşa, V., and Varjú, K. (2012). Quasi-phase-matching high-harmonic radiation using chirped THz pulses. Phys. Rev. Lett. *108*, 193903. https://doi.org/10.1103/physrevlett.108.193903.

Kuk, D., Yoo, Y.J., Rosenthal, E.W., Jhajj, N., Milchberg, H.M., and Kim, K.Y. (2016). Generation of scalable terahertz radiation from cylindrically focused two-color laser pulses in air. Appl. Phys. Lett. *108*, 121106. https://doi.org/10.1063/1.4944843.

LaRue, J.L., Katayama, T., Lindenberg, A., Fisher, A.S., Öström, H., Nilsson, A., and Ogasawara, H. (2015). THz-pulse-induced selective catalytic CO oxidation on Ru. Phys. Rev. Lett. *115*, 036103. https://doi.org/10.1103/physrevlett.115.036103.

Li, C., Zhou, M.L., Ding, W.J., Du, F., Liu, F., Li, Y.T., Wang, W.M., Sheng, Z.M., Ma, J.L., Chen, L.M., et al. (2011). Effects of laser-plasma interactions on terahertz radiation from solid targets irradiated by ultrashort intense laser

pulses. Phys. Rev. E *84*, 036405. https://doi.org/10.1103/physreve.84.036405.

Li, X., Qiu, T., Zhang, J., Baldini, E., Lu, J., Rappe, A.M., and Nelson, K.A. (2019). Terahertz field–induced ferroelectricity in quantum paraelectric SrTiO3. Science *364*, 1079–1082. https://doi.org/10.1126/science.aaw4913.

Li, Y., Li, C., Zhou, M., Wang, W., Du, F., Ding, W., Lin, X., Liu, F., Sheng, Z., Peng, X., et al. (2012). Strong terahertz radiation from relativistic laser interaction with solid density plasmas. Appl. Phys. Lett. *100*, 254101.

Liao, G.Q., and Li, Y.T. (2019a). Review of intense terahertz radiation from relativistic laser-produced plasmas. IEEE Trans. Plasma Sci. *47*, 3002–3008. https://doi.org/10.1109/tps.2019.2915624.

Liao, G., Li, Y., Liu, H., Scott, G.G., Neely, D., Zhang, Y., Zhu, B., Zhang, Z., Armstrong, C., Zemaityte, E., et al. (2019b). Multimillijoule coherent terahertz bursts from picosecond laser-irradiated metal foils. Proc. Natl. Acad. Sci. *116*, 3994–3999. https://doi.org/10.1073/pnas.1815256116.

Liao, G.Q., Li, Y.T., Li, C., Su, L.N., Zheng, Y., Liu, M., Wang, W.M., Hu, Z.D., Yan, W.C., Dunn, J., et al. (2015). Bursts of terahertz radiation from large-scale plasmas irradiated by relativistic picosecond laser pulses. Phys. Rev. Lett. *114*, 255001. https://doi.org/10.1103/physrevlett.114.255001.

Liao, G.Q., Li, Y.T., Zhang, Y.H., Liu, H., Ge, X.L., Yang, S., Wei, W.Q., Yuan, X.H., Deng, Y.Q., Zhu, B.J., et al. (2016). Demonstration of coherent terahertz transition radiation from relativistic laser-solid interactions. Phys. Rev. Lett. *116*, 205003. https://doi.org/10.1103/physrevlett.116.205003.

Liao, G.-Q., Liu, H., Scott, G.G., Zhang, Y.-H., Zhu, B.-J., Zhang, Z., Li, Y.-T., Armstrong, C., Zemaityte, E., Bradford, P., et al. (2020). Towards terawatt-scale spectrally tunable terahertz pulses via relativistic laser-foil interactions. Phys. Rev. X *10*, 031062. https://doi.org/10.1103/physrevx.10.031062.

Mondal, S., Wei, Q., Ding, W.J., Hafez, H.A., Fareed, M.A., Laramee, A., Ropagnol, X., Zhang, G., Sun, S., Sheng, Z.M., et al. (2017). Aligned copper nanorod arrays for highly efficient generation of intense ultra-broadband THz pulses. Sci. Rep. *7*, 40058. https://doi.org/10.1038/srep40058.

Nanni, E.A., Huang, W.R., Hong, K.H., Ravi, K., Fallahi, A., Moriena, G., Dwayne Miller, R.J., and Kartner, F.X. (2015). Terahertz-driven linear electron acceleration. Nat. Commun. *6*, 8486. https://doi.org/10.1038/ncomms9486.

Ouyang, C., Li, S., Ma, J., Zhang, B., Wu, X., Ren, W., Wang, X., Wang, D., Ma, Z., Wang, T., et al. (2021). Terahertz strong-field physics in light-emitting diodes for terahertz detection and imaging. Commun. Phys. *4*, 5. https://doi.org/10.1038/s42005-020-00508-w.

Pacey, T.H., Saveliev, Y., Healy, A., Huggard, P.G., Alderman, B., Karataev, P., Fedorov, K., and Xia, G. (2019). Continuously tunable narrow-band terahertz generation with a dielectric lined waveguide driven by short electron bunches. Phys. Rev. Accel. Beams *22*, 091302. https://doi.org/10.1103/physrevaccelbeams.22.091302.

Ping, Y., Shepherd, R., Lasinski, B.F., Tabak, M., Chen, H., Chung, H.K., Fournier, K.B., Hansen, S.B., Kemp, A., Liedahl, D.A., et al. (2008). Absorption of short laser pulses on solid targets in the ultrarelativistic regime. Phys. Rev. Lett. *100*, 085004. https://doi.org/10.1103/physrevlett.100.085004.

Ramis, R., Eidmann, K., Meyer-ter-Vehn, J., and Hüller, S. (2012). MULTI-fs–A computer code for laser–plasma interaction in the femtosecond regime. Comput. Phys. Commun. *183*, 637–655. https://doi.org/10.1016/j.cpc.2011.10.016.

Roeder, F., Shalaby, M., Beleites, B., Ronneberger, F., and Gopal, A. (2020). THz generation by optical rectification of intense near-infrared pulses in organic crystal BNA. Opt. Express *28* (24), 36274–36285. https://doi.org/10.1364/oe.404690.

Schroeder, C.B., Esarey, E., van Tilborg, J., and Leemans, W.P. (2004). Theory of coherent transition radiation generated at a plasma-vacuum interface. Phys. Rev. E *69*, 016501. https://doi.org/10.1103/physreve.69.016501.

Shan, J., Weling, A.S., Knoesel, E., Bartels, L., Bonn, M., Nahata, A., Reider, G.A., and Heinz, T.F. (2000). Single-shot measurement of terahertz electromagnetic pulses by use of electro-optic sampling. Opt. Lett. *25* (6), 426–428. https://doi.org/10.1364/ol.25.000426.

Stojanovic, N., and Drescher, M. (2013). Accelerator-and laser-based sources of high-field terahertz pulses. J. Phys. B Atom. Mol. Opt. Phys. *46* (19), 192001. https://doi.org/10.1088/0953-4075/46/19/192001.

Tanaka, K.A., Yabuuchi, T., Sato, T., Kodama, R., Kitagawa, Y., Takahashi, T., Ikeda, T., Honda, Y., and Okuda, S. (2005). Calibration of imaging plate for high energy electron spectrometer. Rev. Sci. Instrum. *76*, 013507. https://doi.org/10.1063/1.1824371.

Tarekegne, A.T., Hirori, H., Tanaka, K., Iwaszczuk, K., and Jepsen, P.U. (2017). Impact ionization dynamics in silicon by MV/cm THz fields. New J. Phys. *19*, 123018. https://doi.org/10.1088/1367-2630/aa936b.

Tian, Q., Du, Y., Xu, H., Liang, Y., Wang, Y., Tan, Y., Yan, L., Li, R., Cheng, C., Huang, W., and Tang, C. (2020). Single-shot spatial-temporal electric field measurement of intense terahertz pulses from coherent transition radiation. Phys. Rev. Accel. Beams *23*, 102802. https://doi.org/10.1103/physrevaccelbeams.23.102802.

Tonouchi, M. (2007). Cutting-edge terahertz technology. Nat. Photon. *1*, 97–105. https://doi.org/10.1038/nphoton.2007.3.

Vicario, C., Ovchinnikov, A.V., Ashitkov, S.I., Agranat, M.B., Fortov, V.E., and Hauri, C.P. (2014). Generation of 09-mJ THz pulses in DSTMS pumped by a Cr:Mg_2SiO_4 laser. Opt. Lett. *39*, 6632–6635. https://doi.org/10.1364/ol.39.006632.

Wilks, S.C., and Kruer, W.L. (1997). Absorption of ultrashort, ultra-intense laser light by solids and overdense plasmas. IEEE J. Quan. Electron. *33*, 1954–1968. https://doi.org/10.1109/3.641310.

Woldegeorgis, A., Kurihara, T., Almassarani, M., Beleites, B., Grosse, R., Ronneberger, F., and Gopal, A. (2018). Multi-MV/cm longitudinally polarized terahertz pulses from laser–thin foil interaction. Optica *5* (11), 1474. https://doi.org/10.1364/optica.5.001474.

Wu, Z., Fisher, A.S., Goodfellow, J., Fuchs, M., Daranciang, D., Hogan, M., Loos, H., and Lindenberg, A. (2013). Intense terahertz pulses from SLAC electron beams using coherent transition radiation. Rev. Sci. Instrum. *84*, 022701. https://doi.org/10.1063/1.4790427.

Yang, X., Vaswani, C., Sundahl, C., Mootz, M., Luo, L., Kang, J.H., Perakis, I.E., Eom, C.B., and Wang, J. (2019). Lightwave-driven gapless superconductivity and forbidden quantum beats by terahertz symmetry breaking. Nat. Photon. *13*, 707–713. https://doi.org/10.1038/s41566-019-0470-y.

Yu, P.Y., and Cardona, M. (2010). Fundamentals of Semiconductors: Physics and Materials Properties (Springer Science and Business Media).

Zhang, B., Ma, Z., Ma, J., Wu, X., Ouyang, C., Kong, D., Hong, T., Wang, X., Yang, P., Chen, L., et al. (2021). 1.4-mJ high energy terahertz radiation from lithium niobates. Laser Photon. Rev. *15*, 2000295. https://doi.org/10.1002/lpor.202000295.

Zhang, D., Fallahi, A., Hemmer, M., Wu, X., Fakhari, M., Hua, Y., Cankaya, H., Calendron, A.L., Zapata, L.E., Matlis, N.H., et al. (2018). Segmented terahertz electron accelerator and manipulator (STEAM). Nat. Photon. *12*, 336–342. https://doi.org/10.1038/s41566-018-0138-z.

STAR★METHODS

KEY RESOURCES TABLE

REAGENT or RESOURCE	SOURCE	IDENTIFIER
Chemicals, peptides, and recombinant proteins		
Copper foil	Goodfellow	CAS # 7440-50-8
Software and algorithms		
EPOCH	Arber et al. (2015)	https://iopscience.iop.org/article/10.1088/0741-3335/57/11/113001/meta
MULTI	Ramis et al., 2012	https://doi.org/10.1016/j.cpc.2011.10.016
Casino 2	Université de Sherbrooke	https://www.gel.usherbrooke.ca/casino/index.html

RESOURCE AVAILABILITY

Lead contact

Further information and requests for resources and reagents should be directed to and will be fulfilled by the lead contact, Guo-Qian Liao(gqliao@iphy.ac.cn).

Materials availability

This study did not generate new unique reagents.

Data and code availability

The data are available upon reasonable request by contacting the lead contact.

This paper does not report original code.

Any additional information required to reanalyze the data reported in this paper is available from the lead contact upon request.

EXPERIMENTAL MODEL AND SUBJECT DETAILS

Our study does not use experimental models typical in the life sciences.

METHOD DETAILS

Terahertz waveform measurement

Terahertz time-domain waveform was measured using the single-shot non-colinear electro-optic (EO) sampling method (Shan et al., 2000). A 100 μm thick <110 > cut gallium phosphide (GaP) crystal was placed at the second focus of the ellipsoidal mirror as the EO crystal. A small portion of the main laser beam was used as the probe. The probe laser beam splitter, delay line, and the GaP crystal were all placed in the vacuum chamber to ensure the minimum pulse duration of the probe. The terahertz beam was normally incident onto the EO crystal, inducing birefringence of the probe beam. As the probe laser pulse was 45° incident onto the EO crystal, different part of the laser beam arrived on the crystal at different time, thus encoding the time-domain information of the terahertz radiation into the spatial distribution of the probe laser beam. The temporal resolution is given as $\Delta t = \frac{w_{pixel}*\tan(\alpha)}{c}$, where w_{pixel} is the pixel size of the detection CCD, α is the incident angle of the probe beam, and c is the speed of light. In our experimental setup, Δt was calculated to be 18 fs. Considering the 30-fs probe laser pulse duration, the temporal resolution was 30fs in our experiment. The total time window $t_{total} = \frac{w*\tan(\alpha)}{c}$, where w is the transverse size of the probe laser beam on the EO crystal. In our experimental setup, $t_{\text{total}} \sim 4$ps.

The EO signal is determined by the phase retardation of the probe laser. The phase retardation is given by (Tian et al., 2020) $\Gamma = \frac{2\pi l n_0^3 r_{41} E_{THz}}{\lambda_0 \sqrt{\eta}\cos\theta}$, where l is the thickness of the crystal, r_{41} and n_0 are the EO coefficient and refractive index of the crystal, λ_0 is the wave length of the probe laser, η is the THz transmission loss, E_{THz} is

the terahertz field strength. The EO signal $I_{sig} = \frac{I_0}{2}(1 - sin\Gamma)$, where I_0 is the background. By comparing the background and the signal, the terahertz field strength can be retrieved.

Electron measurement

The electron measurement was carried out by using Image Plate (IP). A three-layered IP stack was put ~6 cm away from the target rear. The IP stack was covered with a 25-μm thick aluminum foil to shield the visible light and ions. In the terahertz-charge dependence dataset, two lead plates formed a ~3-mm wide slit at the target rear to shield electrons in other direction. A stepping motor stage was used to update the IP stack position after each laser shot. For the total charge measurement, the lead blocker was removed, and both the laser propagation direction and the target normal direction were covered by the IP stack. The signal on the first layer was largely affected by the x-rays emitted from the target rear. The electron temperature was estimated by analyzing the ratio of the signal on the second and the third layer. By comparing with the calculation by the Casino2 Mount-Carlo simulation program and considering an exponential energy spectral distribution of the electrons, the electron temperature was retrieved to be 600 keV. The angular distribution of the electron beam was estimated by the intensity distribution on the second IP layer, and the total charge was estimated after considering the time decay of the signal, the signal reduction by the first IP layer and the total size of the electron spot.

Estimation of terahertz field strength using terahertz-induced absorption bleaching

According to the physical picture of the intervalley scattering, the scattering rate is proportional to the velocity of the electron, $\frac{1}{\tau_{iv}} \propto E_k^{\frac{1}{2}} \propto v_e$. The electron velocity can be expressed as $m^* \frac{dv_e}{dt} = eE_{THz}$. The velocity is proportional to the time integration of the terahertz field, so that the scattering rate is proportional to the time integration of the terahertz electric field as $\frac{1}{\tau_{iv}} \propto \int E_{THz} dt$, which is approximately proportional to the pulse duration multiplied with the peak field strength for a Gaussian-like terahertz pulse. Considering the same doping concentration, the maximum field strength can be retrieved by comparing the integrated terahertz time-domain waveform. In this way, the terahertz field strength can be quantitatively estimated. The enhancement of transmitted terahertz energy by a factor of 2.3 was achieved at ~0.25 GV/m field strength of the ~1-ps Terahertz pulse in the previous experiment (Zhang et al., 2021).

Simulation setup

The hydrodynamics simulation is carried out using open-source code MULTI. We use a 1D simulation to estimate the plasma density scale length when the main laser arrives. A 800-nm femtosecond laser with the intensity of (1-5)× 10^{15} W/cm^2 is incident on a cold solid target with an initial electron density of about 500 n_c, where n_c is the critical plasma density for the 800-nm laser. The electron density distribution at 12 ps after laser-target interactions was extracted from simulations, and then used to evaluate the plasma density scale length.

The PIC simulation is carried out using the open-source code EPOCH. A 30-fs Gaussian laser pulse with a beam waist of 5 μ m is incident onto a plasma slab with 10μ m in thickness and 60μ m in width at an incidence angle of 45°. A thin plasma layer with an exponential density distribution exists at the target front to represent the preplasma. The maximum electron density is set to be 20 n_c and the minimum density is 0.002 n_c. The 60 μ m× 60μ m simulation box is divided to 2400× 2400 cells with 16 particles per cell. The ion charge and mass in the simulations are set to be the parameters of fully ionized copper ions. The energy of charged particles in the simulation box was treated as the absorbed laser energy and the energy portion of forward electrons was obtained by summing up the kinetic energy of electrons propagating inward the target at ~55 fs after the laser peak leaves the target.

QUANTIFICATION AND STATISTICAL ANALYSIS

Our study doesn't include quantification or statistical analysis.